# remote sensing

*Article*

# The S-NPP VIIRS Day-Night Band On-Orbit Calibration/Characterization and Current State of SDR Products

**Shihyan Lee [1,*], Kwofu Chiang [2], Xiaoxiong Xiong [3], Chengbo Sun [2] and Samuel Anderson [2]**

[1] Earth Resource Technology Inc., 14401 Sweitzer Lane, Laurel, MD 20707, USA
[2] Sigma Space Corporation, 4600 Forbes Blvd., Lanham, MD 20706, USA;
    E-Mails: Vincent.Chiang@ssaihq.com (K.C.); Chengbo.Sun@ ssaihq.com (C.S.);
    Samuel.Anderson@ ssaihq.com (S.A.)
[3] NASA Goddard Space Flight Center, Greenbelt, MD 20661, USA;
    E-Mail: Xiaoxiong.Xiong.1@gsfc.nasa.gov

* Author to whom correspondence should be addressed; E-Mail: shihyanlee@yahoo.com;
  Tel.: +617-947-1605; Fax: +301-361-0645.

**Abstract:** The launch of VIIRS on-board the Suomi-National Polar-orbiting Partnership (S-NPP) on 28 October 2011, marked the beginning of the next chapter on nighttime lights observation started by the Defense Meteorological Satellite Program's (DMSP) OLS sensor more than two decades ago. The VIIRS observes the nighttime lights on Earth through its day-night band (DNB), a panchromatic channel covering the wavelengths from 500 nm to 900 nm. Compared to its predecessors, the VIIRS DNB has a much improved spatial/temporal resolution, radiometric sensitivity and, more importantly, continuous calibration using on-board calibrators (OBCs). In this paper, we describe the current state of the NASA calibration and characterization methodology used in supporting mission data quality assurance and producing consistent mission-wide sensor data records (SDRs) through NASA's Land Product Evaluation and Analysis Tool Element (Land PEATE). The NASA calibration method utilizes the OBCs to determine gains, offset drift and sign-to-noise ratio (SNR) over the entire mission. In gain determination, the time-dependent relative spectral response (RSR) is used to correct the optical throughput change over time. A deep space view acquired during an S-NPP pitch maneuver is used to compute the airglow free dark

offset for DNB's high gain stage. The DNB stray light is estimated each month from new-moon dark Earth surface observations to remove the excessive stray light over the day-night terminators. As the VIIRS DNB on-orbit calibration is the first of its kind, the evolution of the calibration methodology is evident when the S-NPP VIIRS's official calibrations are compared with our latest mission-wide reprocessing. In the future, the DNB calibration methodology is likely to continue evolving, and the mission-wide reprocessing is a key to providing consistently calibrated DNB SDRs for the user community. In the meantime, the NASA Land PEATE provides an alternative source to obtain mission-wide DNB SDR products that are calibrated based on the latest NASA DNB calibration methodology.

## 1. Introduction

The VIIRS on the Suomi-National Polar-orbiting Partnership (S-NPP) is a bridge mission between NASA's Earth Observing System (EOS) and the Joint Polar-Orbiting Satellite System (JPSS) [1,2]. One of the new additions on the VIIRS instrument relative to the EOS missions is the day-night band (DNB), a visible and near-infrared panchromatic band that is capable of making observations during both day and night. The VIIRS DNB is designed to improve upon the global nighttime lights observations initiated more than two decades ago by the Defense Meteorological Satellite Program's (DMSP) Operational Linescan System (OLS) [3–5]. Compared to the OLS sensor, the updated optical and electronic systems in VIIRS DNB provide a much-improved spatial and radiometric sensitivity [6,7] and can be continuously calibrated by the on-board calibrators (OBCs) to maintain radiometric accuracy [8]. As a polar orbiting sensor, the VIIRS DNB completes an Earth surface observation twice a day, once during the day and once at night, at a near consistent ground resolution of 750 m. The official DNB data are processed by the Joint Polar Satellite System's (JPSS) Interface and Data Processing Segment (IDPS) and are made available along with all other VIIRS data products in near-real time for all users [9]. With the DNB on S-NPP and its subsequent JPSS missions, our understanding of the Earth's environment and human activities will grow exponentially as more users at all levels benefit from the operationally-produced and publically-available high-quality nighttime light data [10].

The long-term scientific value of the VIIRS DNB sensor relies on a data product that is not only accurately calibrated, but also consistently generated with the best available methodology over time. The VIIRS DNB sensor is the first of its kind to provide on-orbit radiometric calibration. DNB calibration is inherently complicated, due to the sensor's large dynamic range, ultra-high sensitivity, scan-angle-dependent field of view (FOV) and sensitivity to stray light contamination [8,11]. Due to its complexity and novelty, the DNB calibration methodology has evolved over time [6,8,11,12] and is expected to continue to improve as our understanding of the DNB sensor improves. As we update our DNB calibration methodology, it is important that historical data be reprocessed using the same methodology to maintain data continuity. To best serve the user community, the NASA VIIRS Characterization Support Team (VCST) has developed a DNB calibration suite, which incorporates the
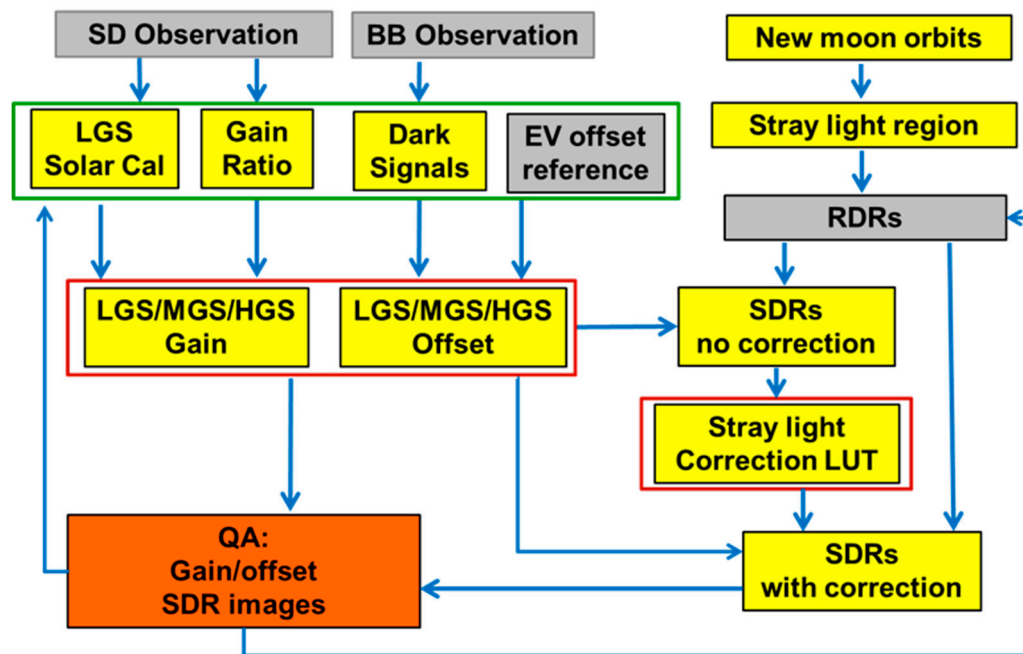
newest calibration strategies into a stand-alone calibration framework. The calibration suite is capable of generating the mission-wide calibration look-up tables (LUTs) efficiently, and we currently are partnering with NASA Land Product Evaluation and Analysis Tool Element (Land PEATE) to reprocess historical data when a major update in DNB calibration occurs. The sensor data records (SDRs) reprocessed by Land PEATE are made publically available through its Level 1 and Atmosphere Archive and Distribution System (LAADS).

The goal of the NASA VCST and Land PEATE (re)processing effort is to facilitate nightlight remote sensing by providing mission-wide DNB SDR products based on the latest calibration methodology and LUTs and to further advance DNB calibration through research and development collaboration. In this paper, we will describe our calibration framework and demonstrate the benefit of having consistent mission-wide calibrated data by examining the calibration consistency and accuracy of existing IDPS DNB products. As the JPSS IDPS currently only focuses on forward processing, the Land PEATE mission-wide reprocessed data products provide an alternative data source for user applications, where calibration consistency and accuracy are of a key priority.

## 2. DNB Calibration Framework

The NASA VIIRS DNB calibration framework is a stand-alone process designed to simplify the anticipated future updates (Figure 1). The radiometric calibration methodology makes use of data continuously collected from VIIRS OBC files to determine the gain and offset parameters over time [8,13]. The DNB sensor consists of four sectors of detectors: one is the low gain stage (LGS), one the intermediate gain stage (MGS) and two redundant arrays, HGA and HGB, are the high gain stage (HGS) [14]. Once each orbit, the LGS gains are computed from Solar Diffuser (SD) observations recorded while the SD is fully illuminated by the Sun. The LGS gains are computed using a time-dependent modulated relative spectral response (RSR) to reflect the optical property change due to the rotating telescope assembly (RTA) mirror degradation (see Section 3.1). SD observations recorded while the SD is not fully illuminated are used to compute cross-stage gain ratios (MGS/HGA, MGS/HGB and LGS/MGS) using signals within the dynamic ranges of both the higher and the lower gain stages. In addition, when the spacecraft is completely within the Earth's shadow, blackbody (BB) observations are used to compute the DNB dark signal for all gain stages. The time series of computed gains, gain ratios and dark signals are saved in history files. These time series of calibration data are then smoothed to reduce random noise before they are used in the production of calibration look-up-tables (LUTs). Currently, the smoothing window of one day is applied to the LGS gain and dark signals, and a 10-day window is used for the gain ratios. Using the smoothed values, the MGS gains are computed from LGS and MGS/LGS gain ratios, and the HGS gains are computed from MGS and the mean of HGA/MGS, HGB/MGS gain ratios. The Earth view (EV) dark offset is determined by using the best known EV dark offset (see Section 3.2) as the reference, adjusted by the BB dark signal drift occurring since the time the EV dark references were measured. The above process determines the calibration gain and offset tables used to produce the calibrated radiance in the SDR products.

**Figure 1.** NASA day-night band (DNB) calibration framework. The red boxes indicate the deliverable or the required look-up tables (LUTs) to generate DNB sensor data records (SDRs). SD, Solar Diffuser; BB, blackbody; LGS, low gain stage; MGS, intermediate gain stage; HGS, high gain stage; EV, Earth view. In the diagram, Cal, Calibration, RDR, Raw Data Record.



A recent addition to the NASA DNB calibration framework is a component to periodically generate a stray light correction LUT (Figure 1) to remove excessive stray light observed while the spacecraft crosses the day-night terminators [11]. During each new moon, the regions of the Earth affected by stray light are determined based on spacecraft solar zenith angle. For certain periods during the new moon, about 14 orbits (one day) of SDRs within and near the stray light contaminated regions are generated without stray light correction. These SDRs are used to estimate the stray light and to produce the stray light correction LUT (see Section 3.3 for details). The stray light correction LUT is then applied within the SDR calibration software to generate a new set of SDRs over the stray-light-affected regions for verification.

Before releasing the LUT to Land PEATE, quality assurance (QA) is performed to ensure that bad data points are investigated and, if needed, removed from gain and offset histories. This may require a reiteration through the whole process to generate a new set of LUTs. The accuracy of the stray light corrections is assessed through analysis of the mean signal residual after correction and visual comparisons between the corrected and the uncorrected SDRs in the same region.

## 3. Radiometric Calibration

### 3.1. Modulated RSR

The NASA DNB radiometric calibration method uses a time-dependent RSR to model the optical change in the mirror property. The S-NPP VIIRS RTA throughput has degraded significantly during the course of on-orbit operations due to unexpected mirror darkening [15]. Because the degradation is
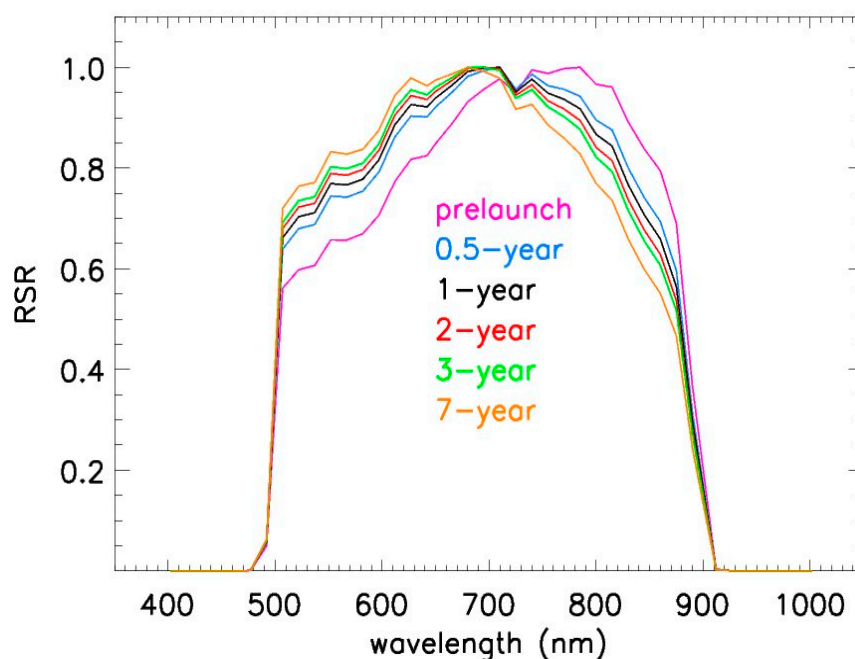
wavelength dependent, it has resulted in a significant change to the DNB RSR within its wide band pass. In DNB radiometric calibration, the RSR is used to determine the proportion of solar irradiance at each spectral wavelength received by the detectors [8]. A change in RSR will affect the total radiance received by the detector. To accurately compute the DNB gains, a time-dependent modulated RSR is used to model the change of incident solar radiance expected during solar calibration events.

Based on the optical throughput degradation model [16], we compute the time-dependent modulated DNB RSR at time *t* as,

$$RSR_{\text{modulated}}(\lambda,t) = \frac{RSR_{original}(\lambda)D(\lambda,t)}{\max(RSR_{original}(\lambda)D(\lambda,t))} \tag{1}$$

In Equation (1), *RSR*modulated is the modulated RSR, *RSRoriginal* is the pre-launch measured RSR and *D* is the degradation factor at wavelength λ and time *t*. Figure 2 shows the pre-launch measured RSR and the computed modulated DNB RSRs at 0.5, 1, 2, 3 and 7 years post-launch based on degradation factors estimated from reflective solar band (RSB) calibration coefficient F-factors [16]. The time series of modulated RSRs show that the relative response has shifted to lower wavelengths over time. The peak response has been lowered from ~790 nm to ~700 nm, and the RSR has increased/decreased for wavelengths under/over 700 nm. The rate of RSR modulation change was fastest in the early months of the S-NPP mission when the throughput degradation was most rapid.
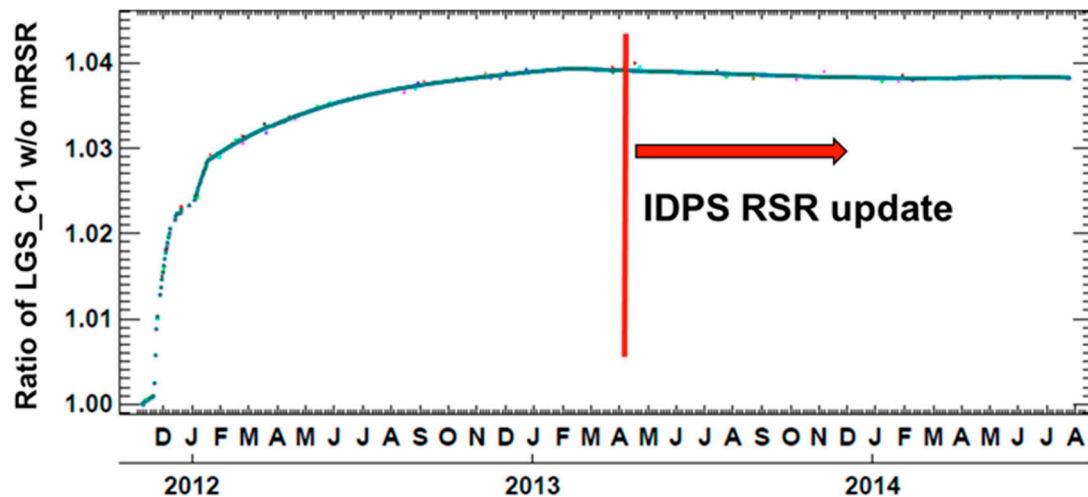
**Figure 2.** Modulated relative spectral responses (RSRs) computed based on current and projected rotating telescope assembly (RTA) mirror degradation trends at selected time intervals.



The calibration biases associated with the DNB RSR modulation can be demonstrated by comparing the gains computed using pre-launch RSR and time-dependent RSRs. Figure 3 shows that the modulated RSR impact on LGS gain has been about 4% since the launch, and three quarters of the total change (~3%) occurred before the DNB CCD reached operational temperature (20 January 2012). The same

modulated RSR impact is expected for the MGS and HGS, as they shared the same optical path as the LGS. To propagate the modulated RSR impact, the MGS and HGS gains are determined from the LGS gains computed with the time-dependent modulated RSR, as well as with the MGS/LGS and HGS/MGS gain ratios.

**Figure 3.** The ratios of LGS gains computed with and without using the time-dependent modulated RSRs. The vertical line indicates the timing of the Interface and Data Processing Segment (IDPS) RSR update.



In April 2013, the JPSS SDR calibration team updated RSR LUTs with modulated RSRs, including DNB, in an offline calibration process to reflect the RSR impact on the calibration coefficients. The IDPS calibration process does not include the capability of time-dependent RSR correction, because the large RTA degradation in S-NPP VIIRS was not anticipated pre-launch [15]. Figure 3 shows that the modulated RSR impact on DNB gain had diminished around the time of the IDPS RSR update. The timing of the RSR update has proven to be adequate for near-term purposes, as the rate of RSR modulation changes are diminishing based on the current projected RSR change (Figure 2). To provide the best radiometric accuracy, the NASA VCST continues to compute DNB gain using the time-dependent RSR and to recommend DNB RSR updates when necessary.
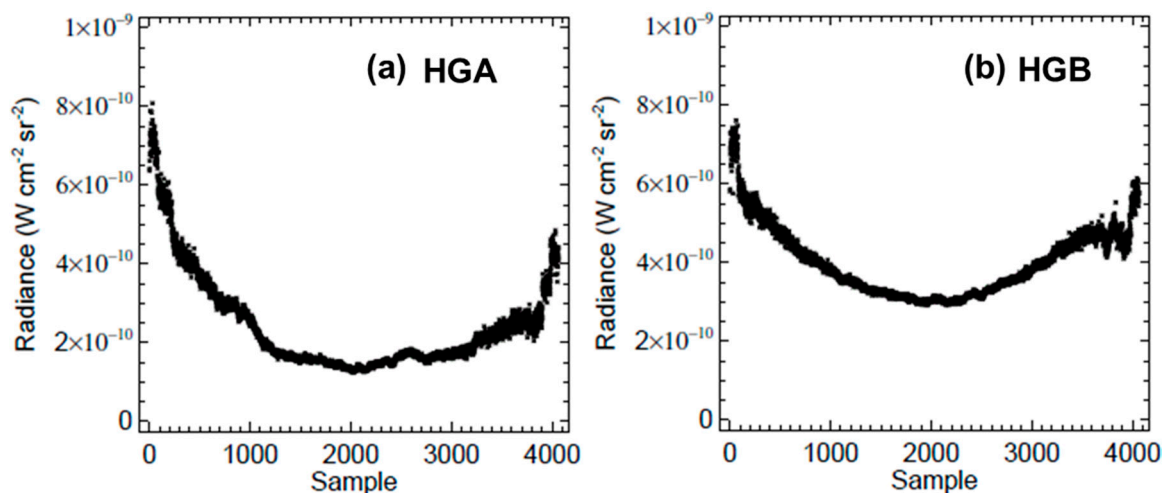
*3.2. EV Dark Offset Reference*

The NASA DNB calibration methodology requires an EV dark offset reference point to determine the time-dependent EV dark offset from the BB dark offset drift [8,13]. The accuracy of the reference EV dark offset is vital, because the errors in the reference offset will be carried over to the entire time series. Currently, the S-NPP flight team performs a special VIIRS recommended operating procedure, VROP702, at the new moon each month to obtain EV dark offset by collecting data over the dark ocean [17]. The dark ocean scene is sufficiently dark for the LGS and MGS, but not for the HGS, due to the effects of airglow. This airglow impact was not anticipated pre-launch partly due to the fact that its magnitude is lower than the DNB's design dynamic range ($3 \times 10^{-9}$ W·cm$^{-2}$·sr$^{-1}$). However, on-orbit analysis has shown that the usable DNB dynamic range is over the design minimum, especially for samples close to

the scan nadir [6] (also see Section 4). An airglow-free EV dark reference is desired for this data collection, because of the superior sensitivity of the DNB detectors.

To establish an airglow-free HGS offset, the deep space scene collected during the S-NPP spacecraft pitch maneuver [18] is used. An S-NPP pitch maneuver was performed during the new moon on 20 February 2012, which was one day before the VIIRS DNB offset determination procedure (VROP702) was performed. During the VROP702, the DNB sensor was commanded to report either HGA or HGB instead of the HGS (mean of HGA and HGB) that it reports during normal operation. During the pitch maneuver, the DNB sensor was configured in normal operational mode, and the HGS data were collected during the maneuver. Figure 4 shows the difference of Earth scene radiance retrieval between VROP702 (looking down at the dark ocean) and pitch maneuver (looking up into deep space). It shows that the VROP702 scene radiance is generally higher than the pitch maneuver scene radiance. The biases are higher for the HGB than for the HGA, and both show a skewed symmetrical pattern with a magnitude from 2 to $8 \times 10^{-10}$ W·cm$^{-2}$·sr$^{-1}$. The airglow is stronger at higher scan angles where longer atmospheric path radiance is collected. The higher HGB-HGS biases are likely the result of stronger airglow within the VROP702's HGB collection region than within the HGA collection region [17].

**Figure 4.** The radiance difference between the pitch maneuver deep space view (performed on 20 February 2012) and the VROP702 (VIIRS recommended operating procedure) dark ocean view (performed on 21 February 2012). (**a**) VROP702 HGA-pitch HGS; (**b**) VROP702 HGB-pitch HGS. Plots show detector averaged biases; the detector dependent airglow intensity could be higher or lower.



### 3.3. Gain and Offset Trending

The partnership between NASA VCST and Land PEATE provides users with mission-wide calibrated DNB data based on the latest calibration algorithm. Here, we show the mission-wide gain and offset used in the latest Land PEATE reprocessed DNB SDRs [19] and compare them with the gain and offset used in the existing IDPS DNB data products. The comparisons for LGS, MGS and HGS are shown in Figures 5–7, respectively.

The trending for the LGS gain (Figure 5a) shows that the gain has gradually increased over time due to the RTA mirror darkening and the spectral shifts in the DNB sensor's RSR. Except for a short period

before the DNB sensor reached operational temperature (20 January 2012) and its gradually increasing trend, the gain appears quite stable over time. In comparison, the IDPS gains are very close to our LGS gains after the April 2013, RSR update. Before the update, the IDPS gains are lower and have several jumps. The discontinuities in the IDPS gains show the evolution of DNB offline calibration methodology. Each time an improvement is made in the calibration methodology, a discontinuity in the absolute radiometric gain is often unavoidable. Such updates are not likely to affect imagery quality, as gains for all detectors and gain modes are shifted proportionally. After the RSR update, a sudden jump in IDPS gain can be seen from May to June of 2014. A solar eclipse during SD calibration event was likely the cause of the jump in the gain. The data points affected by the solar eclipse are removed in our LGS gain history file during the QA process because solar irradiance measurements made during a solar eclipse are invalid for the purposes of calibration. The LGS offset trending (Figure 5b) indicates that there is virtually no drift over time. Our LGS offsets are consistent with IDPS LGS offsets, indicating that the offset drift observed in the calibrator are the same as that observed from the EV. Note that the IDPS offsets are constant within a month, because they are updated once a month from the VROPs.

**Figure 5.** Comparison of daily averaged LGS gain and offset values between NASA and IDPS. (**a**) LGS gain coefficients (LGS_C1), in units of $W \cdot cm^{-2} \cdot sr^{-1}$; (**b**) LGS offset (LGS_DN0) in digital numbers (DNs). The plots show aggregation Mode 1, Detectors 8 and 16 as an example. VCST, VIIRS Characterization Support Team.
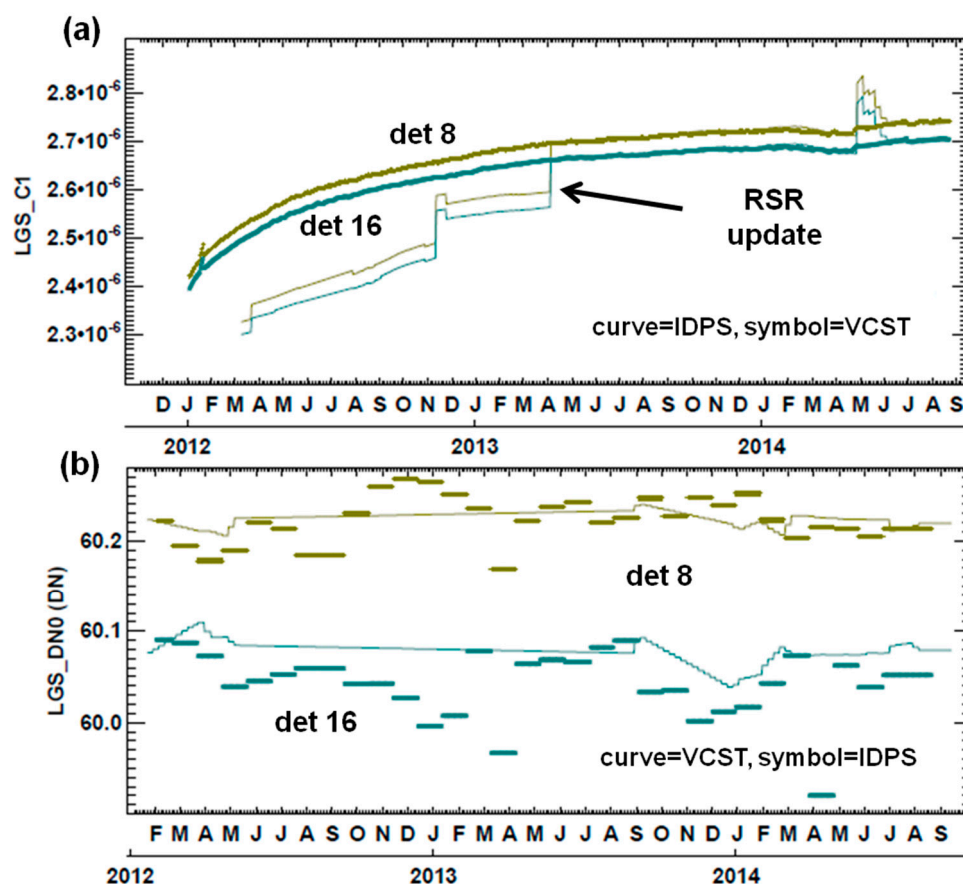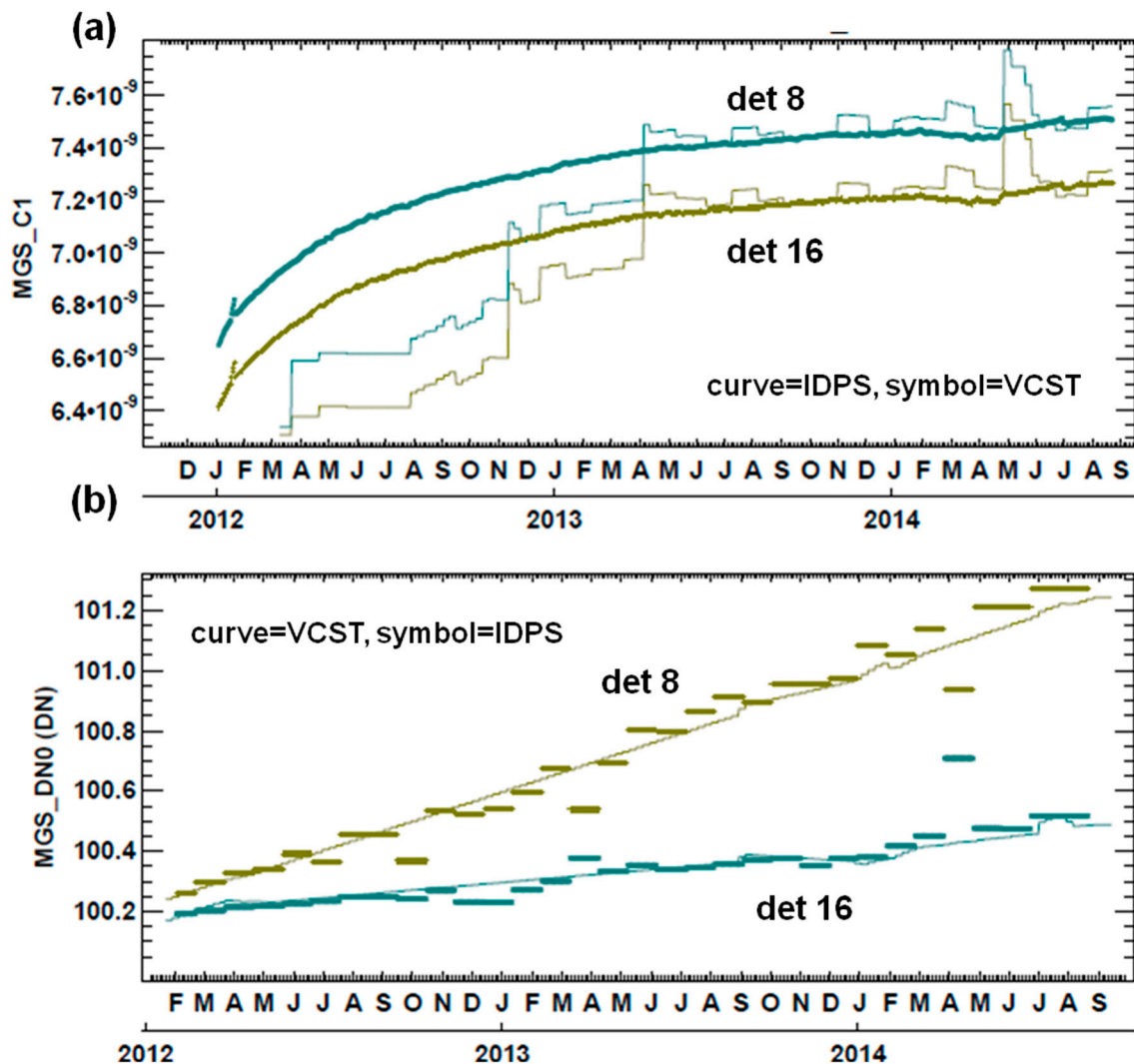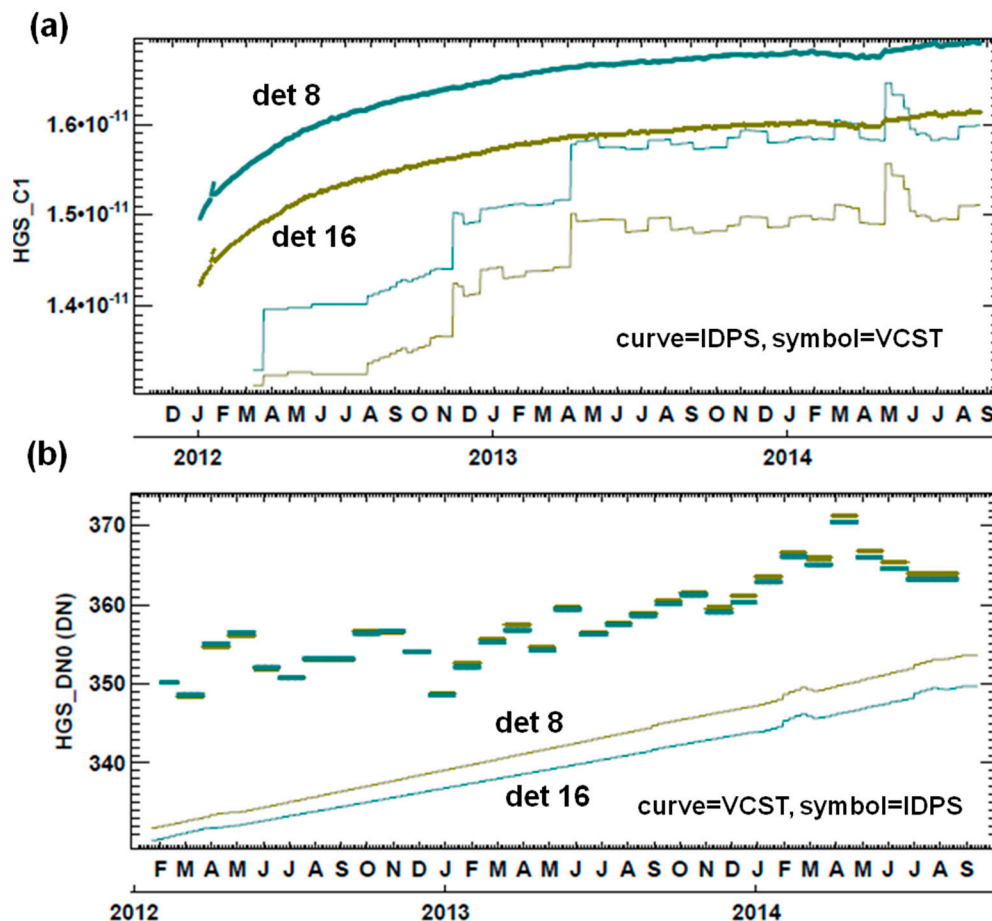
**Figure 6.** Comparison of daily averaged MGS gain and offset values between NASA and IDPS. (**a**) MGS gain coefficients (MGS_C1), in units of $W \cdot cm^{-2} \cdot sr^{-1}$; (**b**) MGS offset (MGS_DN0) in DNs. The plots show aggregation Mode 1, Detectors 8 and 16 as an example.



The MGS gain trending (Figure 6a) shows a gradual increase over time that is similar to what was observed in the LGS gain trending. Since MGS gain is computed from LGS gain and MGS/LGS gain ratios, the results indicate that the MGS/LGS gain ratios have remained relatively constant over time [8]. The IDPS MGS gains show a general trend that is similar to IDPS LGS gain with additional monthly fluctuation. Despite the monthly fluctuation, IDPS MGS gains are fairly consistent with our results after the RSR update (April 2013), except for the spurious LGS gains during May to June of 2014. The monthly discontinuity is caused by the monthly update in MGS/LGS gain ratio tables. It has been suggested that the stray light could pose challenges in determining gain ratios using either SD data (our method) and the Earth scene data (IDPS method) [8,20]. Although it is difficult to verify, we believe that a gradual and predicable MGS gain drift over time should be more accurate. The MGS offset trending (Figure 6b) shows a very slow increase of about 0.4 digital number (DN) counts per year. The IDPS MGS offsets track our values very well despite the fact that they are only updated once a month.

**Figure 7.** Comparison of daily average HGS gain and offset values between NASA and IDPS. (**a**) HGS gain coefficients (HGS_C1), in units of $W \cdot cm^{-2} \cdot sr^{-1}$; (**b**) HGS offset (HGS_DN0) in DNs. The plots show aggregation Mode 1, Detectors 8 and 16 as an example.



The HGS gain (Figure 7a) also follows a general upward trend similar to the MGS and LGS gains, but with some small fluctuations over time. The IDPS HGS gains show a trend that is similar to its MGS gains, where discontinuities are apparent due to the monthly gain ratio updates. After the RSR updates, our HGS gains are about 6%–7% higher than those in the IDPS LUT. The differences are attributable mainly to the HGS/MGS gain ratios, since the MGS gains of the two calibration products are very similar. Studies have suggested the disproportionate levels of stray light on the MGS and HGS detectors during cross-stage calibration as the possible cause of this discrepancy [8,20]. More research is needed for future improvement in HGS gain accuracy. The HGS offset (Figure 7b) shows a gradually increasing trend over time of about six DN per year. The monthly updated IDPS HGS offsets are higher and appear to fluctuate over time, while having the same general upward trend as our HGS offset trends. Since our HGS offset is trended by BB observations and from deep space scenes recorded during an S-NPP pitch maneuver, both of which are free of airglow, the HGS offset comparison may indicate the variation in airglow intensity during each month's offset determination.
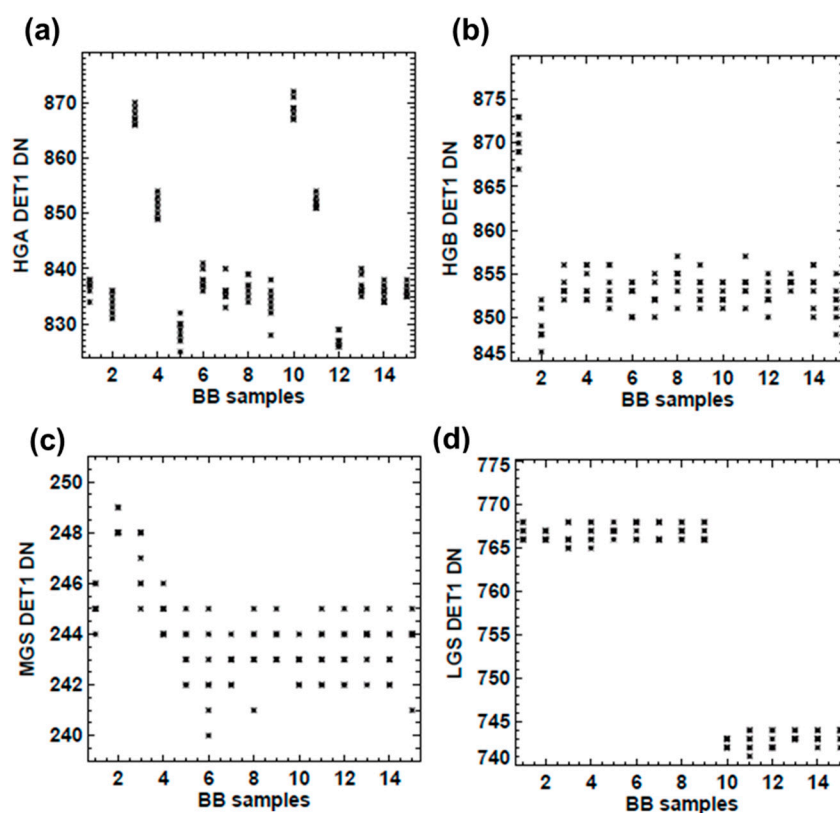
The gain and offset comparisons highlight the progress acquired in our knowledge of how to best calibrate the ultra-sensitive DNB sensor on S-NPP VIIRS. It shows the advantage of using the pitch maneuver and BB observations to determine HGS offset and the impact of the modulated RSR on the gain. It also indicates the need for further research on improving gain determination, especially for the

HGS, which is used for most of the nighttime observations. Finally, the results show the need for reprocessing using calibration coefficients generated based on the most updated method if consistent data are desired.

*3.4. SNR and White Noise*

White noise and signal-to-noise ratio (SNR) estimates derived from statistical analyses of DNB calibration data are characterized and trended to monitor the DNB performance. The DNB sensor collects 15 usable samples for each calibration sector for all four gain stages (HGA, HGB, MGS and LGS). It is assumed that the signals are stationary during the very short 15-sample collection time (approximately 2 ms, depending on aggregation mode). Because the DNB calibration view offsets are sample dependent, the sample offset patterns need to be determined before the noise can be estimated from the sample variance. Figure 8 shows an example of a dark offset pattern generated via data collected from successive dark scans. This offset pattern is caused by a limitation in the DNB sensor's electronics timing card and varies by detector, gain stage and aggregation mode, but is independent of calibration view and the half-angle-mirror (HAM) side. Computing sample noise without removing this fixed pattern will result in artificially increased noise estimates.

**Figure 8.** Repeat DNB measurement of DN at each BB sample during orbit 6600 (4 February 2013, 13:23 UTC) when the spacecraft is on the dark side of the Earth. HGA, HGB, MGS and LGS are shown from (**a**) to (**d**). The repeated dark measurements show a fixed pattern behavior that is different across gain stages. The plots show aggregation Mode 26, Detector 1 as an example, and the fixed pattern is different at different aggregation modes and detectors.

Before computing the sample variance, the DNB calibration view dark offset sample patterns are determined from data collected from the BB while the spacecraft is within the Earth's shadow. The offset sample patterns are determined for a given day for each detector, gain stage and aggregation mode. Using the estimated calibration view sample offsets, we can compute the background subtracted DN for each DNB calibration view sample. We then compute the DNB noise from the variance of the 15 calibration view samples. The noise is computed as the sample standard deviation of the zero radiance view, and the SNR is computed assuming a mean view radiance of $3 \times 10^{-9}$ W·cm$^{-2}$·sr$^{-1}$, the specified minimum DNB dynamic range.

Figure 9 shows the detector-averaged DNB white noise computed using BB dark views for all gain stages and aggregation modes. Figure 10 shows the DNB aggregation mode used for each set of EV samples. The information in Figures 9 and 10 gives an estimate of white noise at each EV sample. The mean values for the months February 2012, and August 2014, are shown as (+) and (*), respectively, in the plots. The DNB white noise has slowly increased over time (results not shown here), and we show the 2012 and 2014 values as snapshots. For white noise in a specific time frame, it is reasonable to interpolate the values from the 2012 and 2014 values. The white noise is lower at the lower aggregation modes near the nadir EV scan angle and gradually increases toward higher aggregation modes near the edge of the EV scan. The redundant high gain stages, HGA and HGB, have similar white noise profiles and increasing trends over time. The white noise measured for the HGA/HGB detectors are ~$0.4 \times 10^{-10}$ to ~$3 \times 10^{-10}$ W·cm$^{-2}$·sr$^{-1}$ from Modes 1 to 32 (nadir to the edge of EV scan) indicating a noise floor that is at least an order of magnitude lower than the design dynamic range ($3 \times 10^{-9}$ W·cm$^{-2}$· sr$^{-1}$). The MGS white noise is ~$0.7 \times 10^{-8}$ to ~$8 \times 10^{-8}$ W·cm$^{-2}$·sr$^{-1}$, and the LGS white noise is ~$0.2 \times 10^{-5}$ to ~$2.3 \times 10^{-5}$ W·cm$^{-2}$·sr$^{-1}$ from the center to the edge of the EV scan. Both MGS and LGS white noise also increased over time, although at a slower rate than the HGA and HGB noise.

Figure 11 shows the detector-averaged SNR for the HGA, HGB and HGS. The mean SNR values for the months February 2012, and August 2014, are shown as (+) and (*), respectively, in the plots. The HGA and HGB SNRs are computed using SV samples when the S-NPP spacecraft is crossing the north-south terminator during the night orbit where the Earth radiance is near the specified SNR radiance of $3 \times 10^{-9}$ W·cm$^{-2}$·sr$^{-1}$. Our estimates show that the SNRs for both HGA and HGB have slowly decreased over time (results not shown here) as indicated by the 2012 and 2014 values. HGA and HGB SNRs decreased at similar rates over time with the lower aggregation modes having slightly larger decreases. The decrease in SNR is expected and is mostly caused by the decrease in detector gain due to RTA mirror darkening [15] and the increase in detector noise over time. Since the DNB's EV high gain stage (HGS) readout is the average of HGA and HGB data, the HGS SNR will be higher than the individual HGA and HGB stages [14]. Because the HGA and HGB data are reported separately in the calibration view, the HGS SNRs were estimated using a standard noise propagation method (Equation (2)):

$$SNR_{HGS=} \frac{1}{(0.5 \times \sqrt{\frac{1}{SNR_{HGA}^2} + \frac{1}{SNR_{HGB}^2}})} \tag{2}$$

**Figure 9.** Detector averaged white noise computed from BB view data during February 2012 (+), and August 2014 (*). HGA, HGB, MGS and LGS are shown from (**a**) to (**d**), respectively. The x-axis indicates the DNB aggregation modes, where Modes 1 to 32 are used to collect data from nadir to the edge of the scan (see Figure 10).
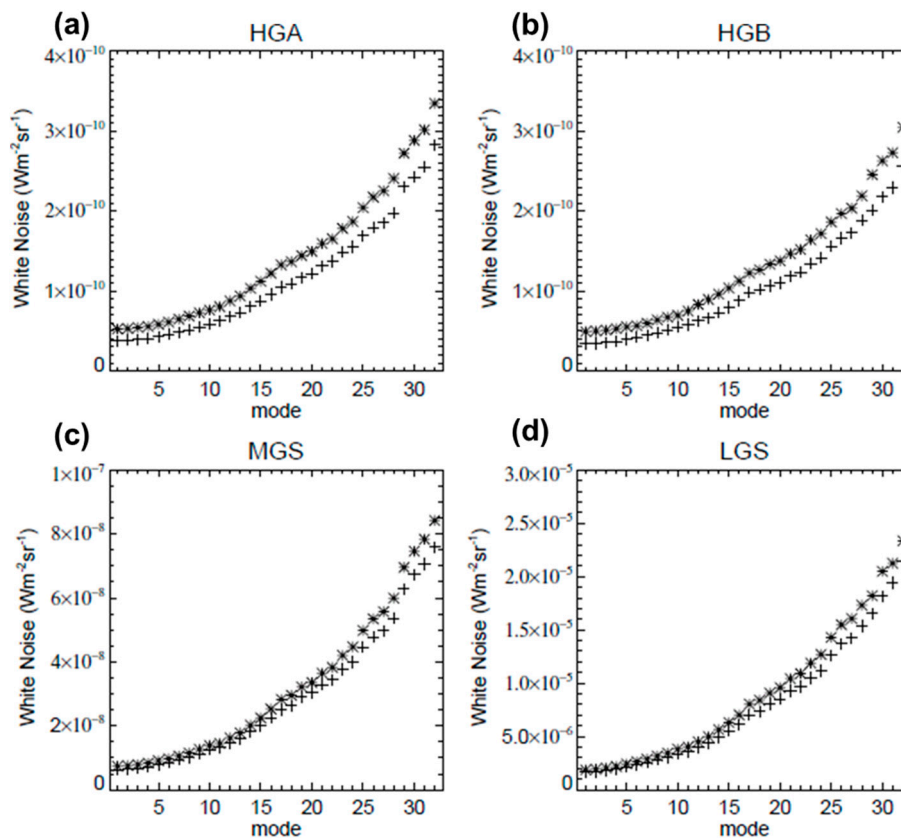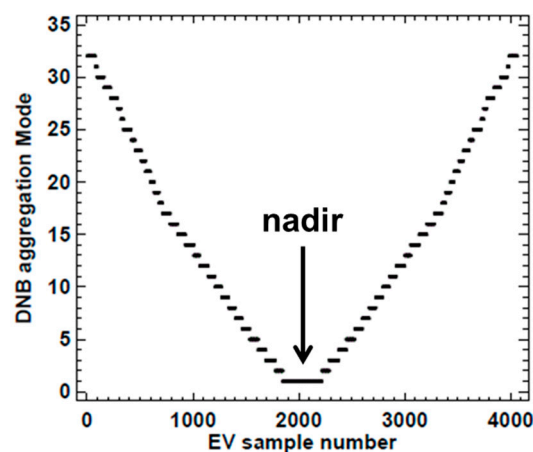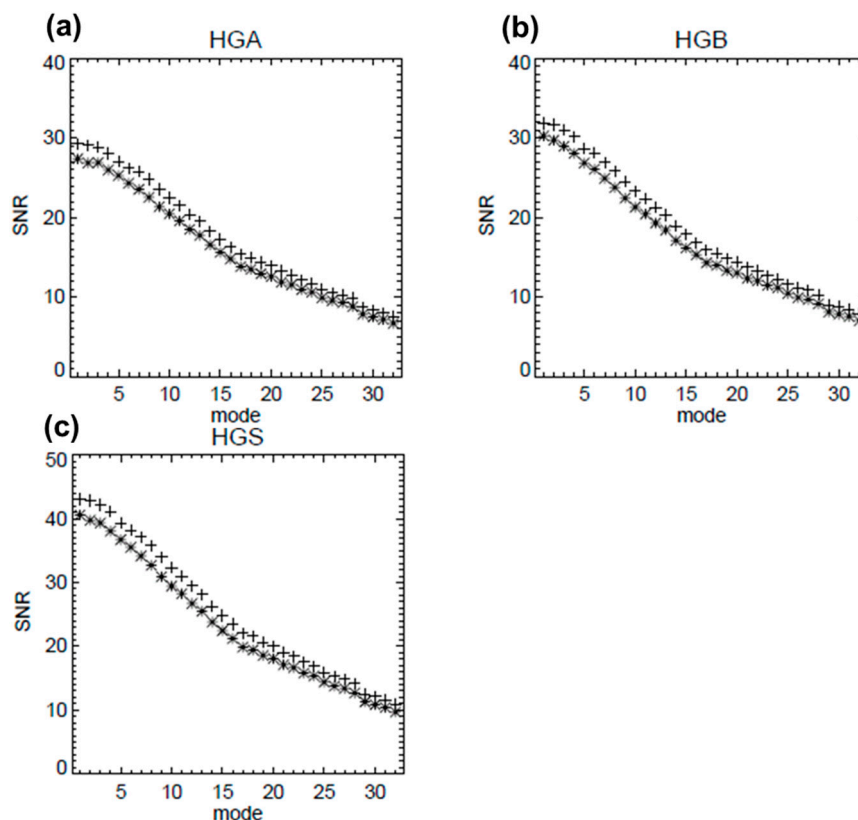


**Figure 10.** DNB aggregation modes *vs*. EV samples. The entire DNB EV consists of 4064 samples from the edge-to-edge scan angle with Sample 2032 centered at the nadir. A total of 32 aggregation modes are used to cover nadir to the edge of the scan angles, with Mode 1 being a nadir mode and Mode 32 at the edge of the scan. The FOV varies among aggregation modes, with Mode 1 being the largest FOV and Mode 32 being the smallest in order to provide near-consistent ground resolution.

The estimated HGS SNRs represent the nominal EV high gain radiometric sensitivity where HGA and HGB data are averaged to produce HGS data. Figure 11 shows that the HGS SNRs are above 40 in the most sensitive nadir aggregation Mode 1 and monotonically decrease to ~10 at the edge aggregation Mode 32. This large change in HGS SNR is due to varying DNB CCD sub-pixel aggregation to achieve the near-constant ground resolution. The minimum usable radiance, therefore, is dependent on scan angle and is much lower than the design specification at nadir. In summary, the DNB data quality is much better at nadir than the edge of the scan. Users should take notice of this characteristic to make full use of DNB data.

**Figure 11.** Detector averaged SNR computed from SV view data for February 2012 (+) and August 2014 (*). HGA, HGB and HGS are shown from (**a**) to (**c**). The x-axis indicates the DNB aggregation modes, where Modes 1 to 32 are used to collect data from nadir to the edge of the EV scan (see Figure 10).



*3.5. Stray Light Correction*

The S-NPP VIIRS DNB on-orbit stray light contamination is larger and wider than was originally expected, with up to 25% of all nighttime data affected. The stray light is caused by the sneak path radiance when the S-NPP spacecraft is illuminated by the Sun and is most prominent while the Earth remains dark. The stray light affects regions covering high latitudes of the Northern and Southern Hemispheres. The magnitude of stray light and the affected latitudes are time dependent, as they are determined by the Earth-Sun-spacecraft geometry. The stray light magnitude also varies by detector, HAM mirror side and RTA position (or scan angle), as the sneak path is different for each detector and

can be modified by HAM mirror and RTA position. A correction algorithm was developed by the IDPS SDR team to estimate the stray light at each new moon [11], and a stray light correction LUT was generated to be incorporated in the DNB SDR calibration algorithm to remove excess stray light. The stray light correction was implemented in the IDPS operational process in August 2013. Because IDPS only performs forward processing, the DNB SDRs prior to August 2013, do not have stray light correction applied. Furthermore, the IDPS operational DNB SDR is generated by using the previous month's stray light correction LUT due to the offline processing latency normally required to apply the new correction LUT into the operational data stream. To remove such a latency constraint, the IDPS has started to apply stray light correction LUTs generated for the same month from the prior year. The updated strategy improves the correction accuracy as the stray light pattern repeats for the yearly Earth-Sun-spacecraft geometry cycle. However, some biases still exist when using the prior year's stray light estimate for correction.

At NASA, we have developed our own stray light correction method and have generated mission-wide stray light correction LUTs. These LUTs were used in Land PEATE Collection 1.1 reprocessing. The NASA DNB stray light correction method is based on the same principles as used in the IDPS method [11], which assumes that the small signal observed over the dark Earth scene during a new moon is the result of a combination of stray light and airglow [21]. Our method, however, is different than the IDPS method in two ways. First, the dark Earth scene signals are computed from up to 14 orbits (one full day) of data during the new moon period, as opposed to the IDPS method, which uses an Earth nighttime light map to mask out the nightlight [11]. In our method, pixels with nightlight are removed as outliers, because repeat measurements at each successive orbit will cover different parts of the Earth. Since nightlights are present in only a small fraction of the Earth's surface, a carefully-selected outlier exclusion threshold can remove most of the contaminated pixels. Secondly, the computed dark scene signals are smoothed over the spacecraft zenith angle and scan angles, except for the region with high contrast, *i.e.*, the penumbra region. In twilight regions, where the Earth scene signals increase exponentially, stray light is assumed to be the same as the last known value as an approximation. Lastly, the airglow in the dark scene is subtracted from regions not affected by the stray light and is subtracted from the dark signals to generate the final stray light estimates. Although we do not attempt to quantify the uncertainty of the corrected radiance, we estimate it to be about half of the scene's airglow variation within the same scan angle. This uncertainty is due to the averaging, smoothing and airglow estimates derived from a region that is likely to have different airglow than the regions affected by stray light.
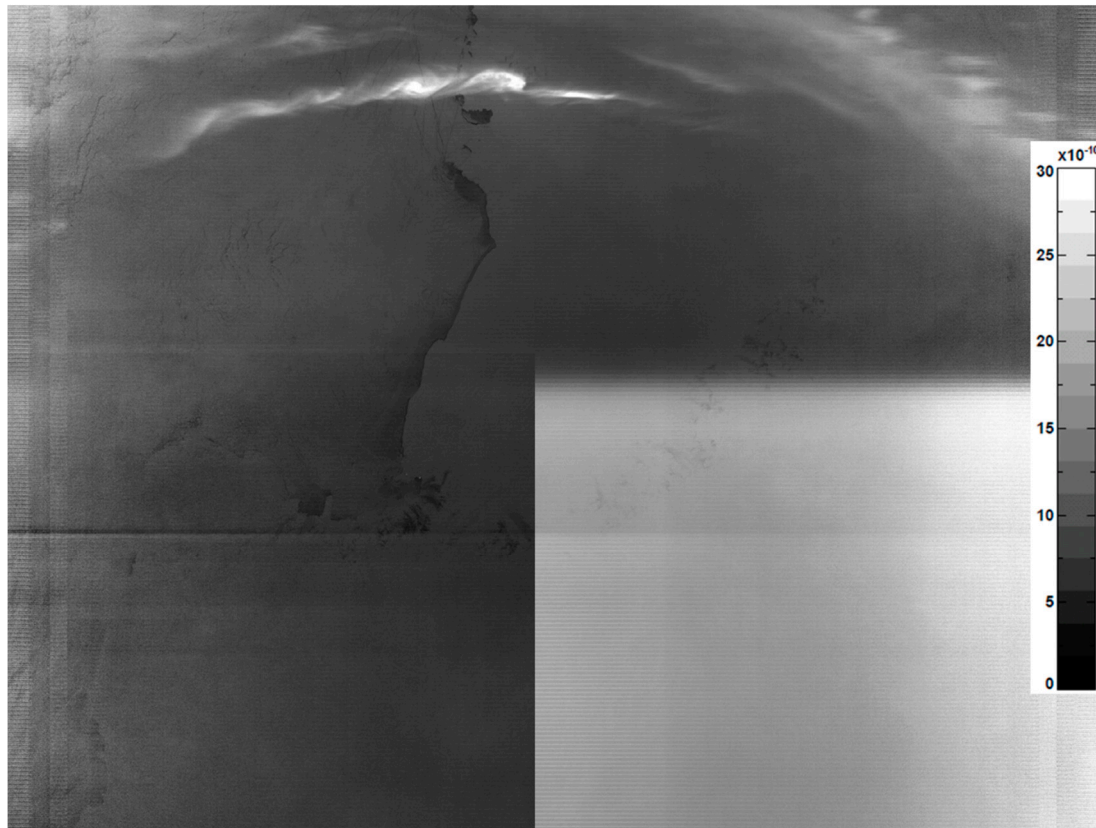
Figure 12 shows an example of a North America DNB SDR image before and after stray light correction. Before the correction (right side of the image), the stray light is visible everywhere north of South Carolina of the United States of America. The apparent striping in the image is the result of strong stray light detector dependency. After the correction (left side of the image), the image is free from stray light contamination without any visible quality degradation of real nightlight features. Note that the latitude of the stray light affected region will change over time as it depends on the Earth-Sun-spacecraft geometry. Because the Earth-Sun-spacecraft geometry roughly repeats at a yearly cycle, the stray light pattern will follow the same cycle. Because of this yearly cycle, it might be a good approximation to use the prior year's stray light correction LUT generated for the same month [21]. However, retroactive verification is necessary, because factors, such as spacecraft altitude, attitude, declination angle drift, *etc.*, might not follow the yearly cycle.

**Figure 12.** An example of Northern Hemisphere DNB SDR image before and after applying stray light correction. The image was taken on 19 June 2012, 07:27 UTC. The legend is in units of W·cm$^{-2}$·sr$^{-1}$.



Figure 13 shows another stray light correction example in the Southern Hemisphere. The uncorrected part of the image (right side in Figure 13) showed that the stray light has a two-tone pattern, which is the result of additional stray light entering through the SD screen, a path that is only possible when the spacecraft is near solar calibration events in the southern day-night terminator crossing. Removing the stray light from the SD path is challenging, because it is more sensitive to the spacecraft azimuth angle than the stray light entering from the EV port. The stray light corrected part of the image (left side in Figure 13) shows that most of the stray light-associated features are removed. However, a dark strip can be observed about 2/3 down in the image that is the result of over-correction. The over-correction is mostly caused by the drift of the SD port stray light onset angle since the stray light correction LUT was generated. The accuracy of the SD port stray light onset angle is important, because the stray light signal has a sharp increase. The mismatched SD port stray light onset angle will result in either over- (in Figure 13 example) or under-correction. Because the SD port stray light onset angle changes at a faster rate than the onset of EV port stray light angle, using the stray light correction LUT derived from the closest new moon data can minimize the SD onset angle differences. In verifying the SD onset angle shifts, we generated test images using stray light correction LUTs from prior months (results not shown here). We found that the area of under-correction increases as the time between the image and correction LUT time. For future improvement, a new LUT format or a different approach is needed to remove the limitations of the current design of the stray light correction mechanism.

**Figure 13.** An example of Southern Hemisphere DNB SDR product before and after applying stray light correction. The image was taken on 19 June 2012, 08:01 UTC. The legend is in units of $W \cdot cm^{-2} \cdot sr^{-1}$.



## 4. Conclusions

In this paper, we discussed the NASA S-NPP VIIRS DNB on-orbit calibration and performance assessment, the improvements made since launch, some remaining challenges and the calibration framework used to generate mission-wide LUTs for Land PEATE reprocessing. As part of our long-term quality assurance, we examine the gain and offset trending, as well as selected SDR images to ensure out-of-family behavior is not caused by calibration artifacts. Our long-term trending also includes comparisons with the official IDPS products as cross-verifications. We expect other forward-processed DNB products, *i.e.*, data produced by NASA atmosphere PEATE, to be similar to IDPS products, and the results presented here can be used to identify potential anomalous data behavior, as well.

Our assessments for the past 2.5 years of S-NPP VIIRS data show that the DNB had performed very well. The trending shows that both the gain and offset have been very stable and have gradually increased over time. The detector white noise has increased at a very slow pace, and the SNR has decreased slightly over time. The gain and noise increases are greater than expected due to the unexpectedly large RTA mirror degradation. The RTA mirror degradation also caused the DNB's RSR to change over time, resulting in additional gain increases. Due to the varying aggregation modes used in acquiring the EV data, the DNB sensitivity is scan angle dependent, and the pixels at scan nadir have the highest sensitivity. Our estimates show a noise floor of about $4 \times 10^{-11}$ $W \cdot cm^{-2} \cdot sr^{-1}$ in the most sensitive nadir pixels, and the noise at the edge-of-scan pixels is about an order of magnitude larger. The noise and SNR

estimates indicate that the minimum usable radiance should approach $10^{-10}$ W·cm$^{-2}$·sr$^{-1}$ in the most sensitive nadir pixels, and the sensitivity should gradually decrease as scan angle increases.

The novelty and challenges in calibrating VIIRS DNB can be shown in the cross-comparison of the latest VCST mission-wide calibration with historical IDPS calibration. The IDPS calibration is based on the most optimal method implemented at the time. As our understanding of DNB calibration has improved, the calibration method is updated, and the results can be seen in the discontinuity in the IDPS calibration long-term trends. The comparison between the VCST and official IDPS calibration shows the potential biases when using the official IDPS data for long-term studies. The results highlight the need for reprocessing to ensure consistent data quality and continuity, which are critical to long-term climate data research.

The VCST implemented DNB stray light correction in early 2014 and created stray light correction LUTs for the entire mission. These LUTs are applied in the latest Land PEATE reprocessing (Collection 1.1) to produce the mission-wide stray light-free DNB SDRs. As the DNB stray light could affect up to 25% of nighttime images, this form of correction significantly increased the amount of usable data, especially for the high latitude regions, where the stray light is persistent year-round.

For calibration of the ultra-sensitive DNB, many more challenges remain. In this paper, we have shown the evolution of the S-NPP VIIRS DNB calibration methodology and development, recommended possible improvements and identified some future research. As we continue to improve the understanding of DNB, the future update on the calibration methodology is inevitable, and the importance of reprocessing will grow each time an update is implemented.

## Acknowledgments

## Author Contributions

Shihyan Lee designed the study, developed the methodology, performed the analysis and wrote the manuscript. Kwofu Chiang and Xiaoxiong Xiong contributed to the design of the study and manuscript reviews. Chengbo Sun collected the data and performed re-analysis for parts of the study. Samuel Anderson developed the software tools that are vital to stray light correction implementation and edited the manuscript.

## Conflicts of Interest

The authors declare no conflict of interest.

## References and Notes

1. Lee, T.F.; Nelson, S.C.; Dills, P.; Riishojgaard, L.P.; Jones, A.; Li, L.; Miller, S.; Flynn, L.E.; Jedlovec, G.; McCarty, W.; *et al*. NPOESS: Next-Generation operational global earth observations. *Bull. Am. Meteorol. Soc.* **2010**, *91*, 727–740.

2. Hillger, D.; Kopp, T;. Lee, T.; Lindsey, D.; Seaman, C.; Miller, S.; Solbrig, J.; Kidder, S.; Bachmeier, S.; Jasmin, T.; *et al*. First-light imagery from Suomi NPP VIIRS. *Bull. Am. Meteorol. Soc.* **2013**, *94*, 1019–1029.

3. Elvidge, C.D.; Baugh, K.E.; Kihn, E.A.; Kroehl, H.W.; Davis, E.R. Relation between satellite observed visible-near infrared emissions, population, and energy consumption. *Int. J. Remote Sens.* **1997**, *18*, 1373–1379.

4. Elvidge, C.D.; Baugh, K.E.; Kihn, E.A.; Kroehl, H.W.; Davis, E.R. Mapping of city lights using DMSP Operational Linescan System data. *Photogramm. Eng. Remote Sens.* **1997**, *63*, 727–734.

5. Southwell, K. Night lights. *Nature* **1997**, *390*, doi:10.1038/36217.

6. Liao, L.B.; Weiss, S.; Mills, S.; Hauss, B. Suomi NPP CIIRS day-night band on-orbit performace. *J. Geophys. Res. Atmos.* **2013**, *118*, 12707–12718.

7. Elvidge, C.D.; Baugh, K.E.; Zhizhi, M.; Hsu, F.-C. Why VIIRS data are superior to DMSP for mapping nighttime lights. *Proc. Asia Pac. Adv. Netw.* **2013**, *35*, 62–19.

8. Lee, S.; McIntire, J.; Oudrari, H.; Schwarting, T.; Xiong, X. A new method for Suomi-NPP SIIRS day-night band on-orbit radiometric calibration. *IEEE Trans. Geosci. Remote Sens.* **2015**, *53*, 324–334.

9. Sullivan, W.J.; Grant, K.D.; Miller, S.W. JPSS IDPS product generation. In Proceedings of AIAA Space Conference and Exposition, Pasadena, CA, USA, 11–13 September 2012.

10. Miller, S.D.; Mills, S.P.; Elvidge, C.D.; Lindsey, D.T.; Lee, T.F.; Hawkins, J.D. Suomi satellite brings to light a unique frontier of nighttime environmental sensing capabilities. *Proc. Nat. Acad. Sci.* **2012**, *109*, 15707–15710.

11. Mills, S.; Weiss S.; Liang K. VIIRS day/night band (DNB) stray light characterization and correction. *Proc. SPIE* **2013**, *8866*, doi:10.1117/12.2023107.

12. Rausch, K.; Houchin, S.; Cardema, J.; Moy, G.; Hass, E.; de Luccia, F.J. Automated calibration of the Suomi National Polar-Orbiting Partnership (S-NPP) Visible Infrared Imaging Radiometer Suite (VIIRS) reflective solar bands. *J. Geophys. Res. Atmos.* **2013**, *118*, 13434–13442.

13. Lee, S.; McIntire, J.; Oudrari, H.; Schwarting, T.; Xiong, X. A new method for suomi-NPP VIIRS on-orbit day night band radiometric calibration. *IEEE Trans. Geosci. Remote Sens.* **2013**, *53*, 324–334.

14. Mills, S. Joint Polar Satellite System (JPSS) VIIRS Radiometric Calibration Algorithm Theoretical Basis Document (ATBD). Available online: http://npp.gsfc.nasa.gov/sciencedocuments/ 20140421/474-00027_ATBD-VIIRS-Radiometric-Calibration_C.pdf (accessed on 1 October 2014).

15. Barrie, J.D.; Fuqua, P.D.; Meshishnek, M.J.; Ciofalo, M.R.; Chu, C.T.; Chaney, J.A.; Moision, R.M.; Graziani, L. Root cause determination of on-orbit degradation of the VIIRS rotating telescope assembly. *Proc. SPIE* **2013**, *8510*, doi:10.1117/12.933276.

16. Lei, N.; Buenther, B.; Wang, Z.; Xiong, X. Modeling SNPP VIIRS reflective solar bands optical throughput degradation and its impacts on the relative spectral response. *Proc. SPIE* **2013**, *8866*, doi:10.1117/12.2024351.

17. Geis, J.; Florio, C.; Moyer, D.; Rausch, K.; De Luccia, F.J. VIIRS Day-Night Band Gain and Offset Determination and Performance. *Proc. SPIE* **2012**, *8510*, doi:10.1117/12.930078.

18. NASA Land PEATE VIIRS Data Products, Collection 1.1. Available online: http://viirsland.gsfc.nasa.gov/Products.html (accessed on 1 October 2014).

19. Butler, J.J.; Xiong, X.; Barnes, R.A.; Patt, F.S.; Sun, J.; Chiang, K. An overview of Suomi NPP VIIRS calibration maneuvers. *Proc. SPIE* **2012**, *8510*, doi:10.1117/12.930993.

20. Mills, S.; Miller, S. VIIRS Day-Night Band (DNB) calibration methods for improved uniformity. *Proc. SPIE* **2014**, *9218*, doi:10.1117/12.2060143.

21. Lee S.; Sun, C.; Chiang K.F.; Xiong X. An overview of NASA VIIRS Day-Night Band (DNB) on-orbit radiometric calibration. *Proc. SPIE* **2014**, *9218*, doi:10.1117/12.2061912.